Journal of The Electrochemical Society, **157** (1) D10-D15 (2010)
0013-4651/2009/157(1)/D10/6/$28.00 © The Electrochemical Society

High Quality Area-Selective Atomic Layer Deposition Co Using Ammonia Gas as a Reactant

Han-Bo-Ram Lee,[a] Woo-Hee Kim,[b] Jeong Won Lee,[b] Jae-Min Kim,[a,*] Kwang Heo,[d] In Chan Hwang,[b] Yongjun Park,[b] Seunghun Hong,[c,d] and Hyungjun Kim[a,,z]**

[a]*School of Electrical and Electronic Engineering, Yonsei University, Seoul 120-749, Korea*
[b]*Department of Material Science and Engineering, Pohang University of Science and Technology, Pohang 790-784, Korea*
[c]*Department of Physics and Astronomy and* [d]*Interdisciplinary Program in Nano-Science and Technology, Seoul National University, Seoul 151-747, Korea*

Atomic layer deposition (ALD) Co was developed using bis(N,N'-diisopropylacetamidinato)cobalt(II) as a precursor and NH_3 as a reactant, producing pure Co thin films with excellent conformality and nanoscale thickness controllability. In addition to NH_3, the Co films were also deposited by using H_2 gas as a reactant. Compared to ALD Co using H_2, the Co thin films deposited by NH_3 showed a higher film quality, a lower resistivity, and a higher density. The Co thermal ALD process was applied to area-selective ALD using an octadecyltrichlorosilane self-assembled monolayer as a blocking layer, which produced 3 μm wide Co line patterns without an etching process.

[DOI: 10.1149/1.3248002]

Manuscript submitted December 12, 2008; revised manuscript received June 18, 2009. Published November 3, 2009.

Cobalt is one of the promising materials for practical applications as well as fundamental studies in nanotechnology. For example, a giant magnetoresistance effect utilizing a Co/Ru multilayer was a scientifically great finding, which produced a technological breakthrough for the development of magnetic recording media.[1] In addition to applications using the magnetic property of Co, e.g., in a nanomagnet,[2] Co has been intensively investigated for nanoscale semiconductor device fabrications such as nanocrystal memories[3,4] and contact materials.[5,6] With device scaling, a highly conformal Co thin-film deposition is required, especially for nanoscale contact fabrication.[7]

Atomic layer deposition (ALD) is considered a promising technique for nanoscale film deposition due to its excellent conformality and atomic thickness controllability. ALD is a suitable technique for the fabrication of nanostructures. For example, Ru, Co, and Ni nanostructures were fabricated using ALD and nanotemplates.[8,9] Even with practical importance, however, the ALD of most transition-metal films is difficult. For some noble metal systems including Ru,[8] Ir,[10] and Pt,[11] oxygen was used as a reactant to deposit pure metal films through oxidative decomposition of the precursors. However, the O_2-based thermal atomic layer deposition (T-ALD) cannot be applied to the deposition of most transition metals. Thus, the choice of a proper reducing agent is important in metal ALD because high quality metal deposition is usually achieved by a complete reduction of the metal precursor during the reaction between the precursor and the reducing agent. For example, hexafluoroacetylacetonate-based precursors were used for metal ALD, with formalin as a reactant for ALD of Cu [12] and Pd.[13] The use of highly reactive plasma reactants such as H_2 and NH_3 plasma was reported for Ti,[14] Ta,[15] and Ru [16] ALD. Compared to T-ALD, however, plasma-enhanced atomic layer deposition (PE-ALD) has several disadvantages, such as the requirement of an additional apparatus for plasma generation and the negative effects of plasma on film properties, such as damage. Previously, a complicated process employing Ni oxide ALD using an oxidant and sequential reduction by H_2 plasma was reported for producing Ni thin films.[17] However, the direct deposition of ALD transition metals including Co and Ni has rarely been reported.

Meanwhile, area-selective atomic layer deposition (AS-ALD) using self-assembled monolayers (SAMs) is attracting great attention due to its simple process, removing expensive patterning processes such as lithography and etching. By SAM coating on a surface, the surface properties can be changed into hydrophobic or hydrophilic according to the end groups of the SAMs. Because ALD proceeds through entire surface reactions, the deposition characteristics are critically dependent on the surface properties of substrates. In many cases, the nucleation of ALD is easy on hydrophilic OH-terminated substrates (e.g., SiO_2), while it is difficult on hydrophobic surfaces (e.g., a CH_3-terminated surface). Due to the differences in nucleation for SAM-modified surfaces toward the ALD reaction, AS-ALD becomes possible. Several groups utilized AS-ALD to various applications such as fuel cell and solar cell fabrications.[18,19] However, previous studies on AS-ALD have been mostly limited to oxides such as ZrO_2,[20,21] HfO_2,[20,22,23] ZnO,[24] and TiO_2.[25] For metal, AS-ALD processes were reported for only Ru,[26] Pt,[11,27] and Ir,[10] which were deposited using O_2 as an oxidant. Overall, AS-ALD has been mostly explored in ALD processes using oxygen or H_2O as reactants, and chloride or methoxide precursors and AS-ALD using NH_3 or H_2 as a reactant have rarely been studied.[28] Especially, AS-ALD during PE-ALD has not been studied to our knowledge.

Recently, we have developed Co PE-ALD using bis(cyclopentadienyl) cobalt ($CoCp_2$) as a metal precursor and NH_3 plasma as a reactant for nanoscale contact applications.[5] From the PE-ALD process, pure Co films with a very low resistivity of 10 μΩ cm were obtained on both H-terminated Si(001) and OH-terminated SiO_2 substrates. However, high quality Co could not be deposited by T-ALD using the same precursor. Previously, T-ALD using bis(N,N'-diisopropylacetamidinato)cobalt(II) [Co(iPr-AMD)$_2$] and H_2 as a reactant was reported.[29] The same group reported more results on ALD Co, mainly focusing on the role of ALD Co as the nucleation and adhesion layer for ALD Cu.[30] In this study, we developed NH_3-based T-ALD of Co using Co(iPr-AMD)$_2$. Compared to T-ALD Co using H_2, the T-ALD Co using NH_3 showed a high film density and a low resistivity. AS-ALD Co was achieved up to 1000 ALD cycles from T-ALD using NH_3 as well as H_2, and Co nucleation on octadecyltrichlorosilane (OTS) was observed only above 1000 cycles due to the thermal degradation of OTS.

Experimental

In this study, a commercial ALD chamber (Quros Plus 150) with a loadlock chamber was used. This system has a double showerhead system for good uniformity. Further information on chamber configuration can be found in our previous report.[8] Co(iPr-AMD)$_2$ was contained in a stainless steel bubbler, and the temperature of the bubbler was maintained at 65°C to obtain a suitable vapor pressure for the ALD process. During the precursor exposure step, the pre-

---

[*] Electrochemical Society Student Member.
[**] Electrochemical Society Active Member.
[z] E-mail: hyungjun@yonsei.ac.kr

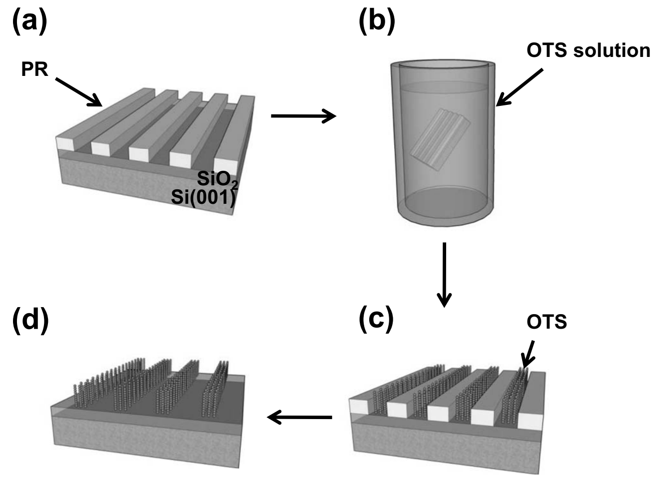

Figure 1. The schematic drawings of preparation sequences for prepatterned OTS: (a) PR patterning on SiO_2 substrate by photolithography, (b) dipping of PR patterned substrate in OTS solution, (c) OTS formation only on PR-free region, and (d) PR removal by acetone of the remaining patterned OTS.

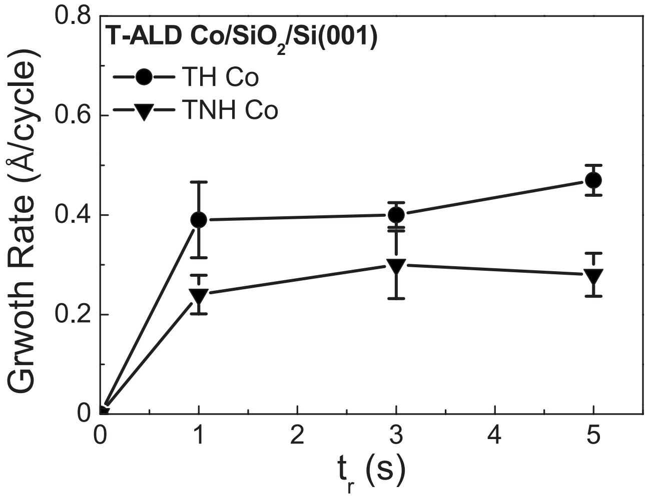

Figure 2. The growth rate vs reactant exposure time of Co T-ALD using $Co(iPr\text{-}AMD)_2$ and two reactants, NH_3 (▼, noted as TNH Co) and H_2 (●, noted as TH Co), on SiO_2 substrate.

cursor vapors were carried into the main chamber by a carrier gas (50 sccm of Ar). For T-ALD Co, two reactants, H_2 and NH_3 gases, were used, and their flows were maintained at 400 sccm. One ALD cycle was composed of four steps consisting of precursor exposure (t_s), purging (t_p), reactant exposure (t_r), and purging, where the flow of Ar purging gas was 50 sccm. t_s and t_p were 3 and 1 s, respectively, and t_r was systematically controlled from 1 to 5 s. Routinely, two kinds of substrates, Si(001) and SiO_2, were used for T-ALD Co. The Si(001) substrates were cleaned by dipping in a buffered oxide etchant (6:1) for 10 s followed by deionized (DI) water rinsing and N_2 blowing, resulting in H-terminated Si. The SiO_2 substrates were cleaned in acetone, isopropyl alcohol, and DI water, followed by N_2 blowing resulting in OH-terminated SiO_2.

For AS-ALD, OTS-coated substrates were prepared. The Si(001) substrate was cleaned by a piranha solution (H_2SO_4:H_2O_2 = 4:1 by volume ratio), resulting in a chemical oxide-coated Si substrate. Subsequently, the Si substrate was dipped in a diluted OTS solution (toluene:OTS = 10 mL:25 μL) for 24 h in a glove box for OTS coating. For the prepatterned OTS coating, the photolithography-assisted process shown in Fig. 1 was employed. The photoresist (PR) (AZ5214) patterning was carried out by photolithography (Fig. 1a) followed by dipping in an OTS solution for 10 min (Fig. 1b), resulting in OTS coating on the PR-free region (Fig. 1c). The coating was performed in a high humidity condition of about 80%, in contrast to the case of blank wafers. Because the water vapors assist in the ordering of OTS, we could coat OTS on the prepatterned substrate for a short time, accompanied with similar hydrophobicity for the case of glove box coating.[31,32] After the PR was removed by acetone, OTS patterns were formed on the SiO_2 substrate (Fig. 1d). After the preparation of OTS-coated substrates, Co T-ALD was performed at 350°C of growth temperature (T_s) and $t_r = 1$ s.

Field-emission-scanning electron microscopy (FESEM) was used for analyses of morphology, and the chemical composition analysis was performed by energy dispersive spectroscopy (EDS) and X-ray photoelectron spectroscopy (XPS). The density and surface morphology of the Co films were analyzed by synchrotron radiation X-ray reflectivity (XRR) (Pohang Acceleration Laboratory, 3C2 beam line) and atomic force microscopy (AFM), respectively. The resistivity of Co films was measured by a four-point probe. The surface hydrophobicity was measured by a static contact angle goniometer (DSA-10, Kruss Co.). For this, 4 μL of water droplets was dropped on a horizontal substrate with an automatic dispensing system, and their contact angles were measured from charge-coupled device camera images. The static contact angles were measured from at least five different sites of a substrate and were averaged. In our study, the OTS-coated substrate showed a contact angle as high as 100°, indicating that the surface was highly hydrophobic, while the uncoated substrate (with chemical oxide) showed a contact angle of less than 20°, agreeing with the previously reported result.[33] The deposition selectivity on patterned OTS substrates was estimated by measuring the thickness difference between OTS-coated and -uncoated regions using a profilometer. Current measurements on AS-ALD Co on a prepatterned OTS surface were carried out using HP 5270A.

Results and Discussion

ALD of Co films using NH_3 and H_2.— In an earlier report on Co ALD using the $Co(iPr\text{-}AMD)_2$ precursor and H_2, a very low growth rate was problematic for practical applications below T_s = 350°C.[29] Thus, we performed Co ALD at a relatively high T_s = 350°C. The Co thin films were deposited by T-ALD using NH_3 (TNH) or H_2 (TH) as a reactant, and the growth characteristics and film properties were comparatively investigated. Figure 2 shows the growth rates of TNH and TH Co films on SiO_2 with increasing t_r from 1 to 5 s. Except for the change in reactants, other process conditions such as T_s, t_r, t_s, and gas flows of the T-ALD were the same for both precursors. The growth rates are saturated at $t_r > 1$ s for both precursors, indicating the self-saturation ALD reactions. However, the saturation growth rate of TH Co (0.43 Å/cycle) is larger than that of TNH Co (0.26 Å/cycle). Meanwhile, the resistivity of TNH Co (~50 μΩ cm) is three to four times lower than that of TH Co (~200 μΩ cm) at $t_r = 5$ s.

The conformality of T-ALD Co was estimated by depositing the films inside nanosize holes. Figure 3a shows the scanning electron microscopy (SEM) image of a hole pattern with a 5:1 aspect ratio (450 nm depth and 90 nm diameter) after 1000 cycles of TNH Co at $t_r = 1$ s. The Co film thicknesses at the top, side wall, and bottom of the pattern are almost the same as 24 nm, resulting in a 100% step coverage. Similarly, the TH Co also produces highly conformal Co films inside the holes, as shown in Fig. 3b. The excellent conformality of both T-ALD processes indicates a saturated surface reaction of ALD, which is consistent with growth rate saturation, as shown in Fig. 2. The SEM images show different surface morphologies of Co films according to the reactants. The TNH Co shows a much larger grain size than TH Co.

The chemical compositions of TNH and TH Co films deposited at $t_r = 5$ s were analyzed by XPS. For TNH Co, narrow XPS peaks are observed in the Co core level at 778.3 and 793.3 eV of binding

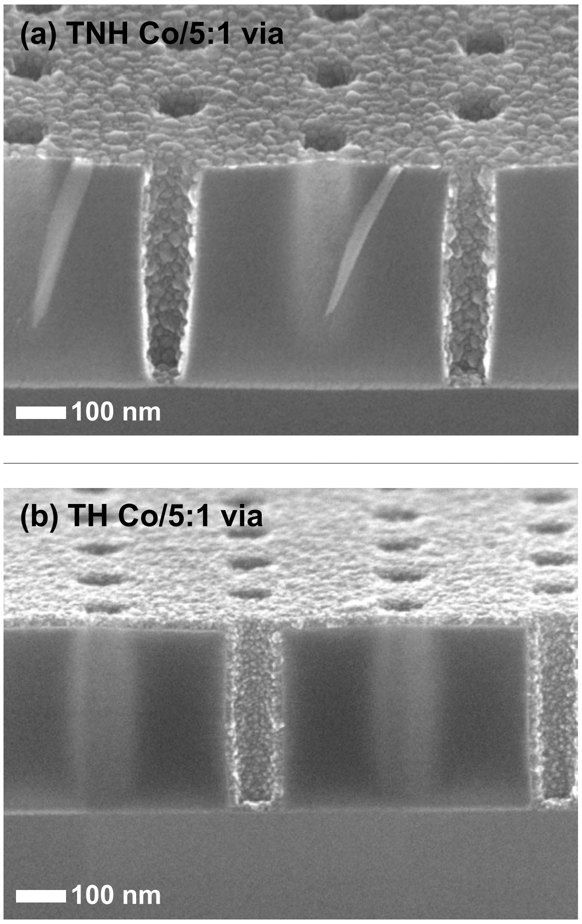

Figure 3. The FESEM images of (a) TNH Co and (b) TH Co films on nanosized hole pattern (450 nm depth and 90 nm diameter).

energy, which correspond to $2p_{3/2}$ and $2p_{1/2}$ peaks of metallic Co (Fig. 4a).[34] The XPS peak intensities related to impurities such as N, O, and C are very weak, as shown in Fig. 4b. In contrast, the Co peaks of the TH Co film shown in Fig. 4c are very broad compared to Fig. 4a. Each of the Co $2p_{3/2}$ and $2p_{1/2}$ peaks is deconvoluted to three peaks denoted by solid, dashed, and dotted lines. The deconvoluted Co $2p_{3/2}$ peaks are observed at 778.3 (solid line), 780.3 (dashed line), and 786.3 eV (dotted line) of binding energy. These peaks correspond to Co–Co bonding, Co–O bonding, and a shake-up satellite peak, respectively, indicating oxidation of the film. It was reported that the shake-up satellite peaks are observed together with the Co–O bonding peak according to oxidation states.[35,36] Indeed, Fig. 4d shows a relatively large O peak. The O XPS peak is mainly observed at 529.7 eV with a small shoulder peak at 531.3 eV, where the high intensity peak corresponds to O–Co bonding, and the small peak corresponds to hydroxyl.[35,36] The molecular structure of the $Co(iPr\text{-}AMD)_2$ is composed of Co atoms directly bonded to four neighboring N atoms without oxygen.[29] Because there is no oxygen atom in the precursor and reactant, the oxygen contamination for TH Co is probably due to postdeposition oxidation. The synchrotron radiation XRR analysis indicates that the film density of TH Co is significantly lower than that of TNH Co (62 vs 79%). Due to the low film density, the oxygen molecules could easily penetrate the TH Co thin films forming a Co–O bond, and the oxidation is exacerbated by the small size grains of TH Co films. Meanwhile, the nitrogen levels are very low in both of the TNH and TH Co films. Thus, the use of NH_3 as a reactant does not significantly increase the level of nitrogen contamination in the film, indicating that the NH_3 molecules effectively cleave the Co–N bonds of the $Co(iPr\text{-}AMD)_2$ forming a pure Co film. Similarly, the deposition of pure Ru by ALD using NH_3 as a reactant was reported previously.[37]

AS-ALD using SAM.— Co T-ALD processes using different reactants, H_2 and NH_3, were applied to AS-ALD. For comparison, we prepared two substrates, OTS-coated and -uncoated substrates, and T-ALD Co was carried out simultaneously on the two samples for 1000 cycles. For TNH Co, SEM and EDS analyses show that the Co film was not deposited onto the OTS-coated surface (Fig. 5a, EDS

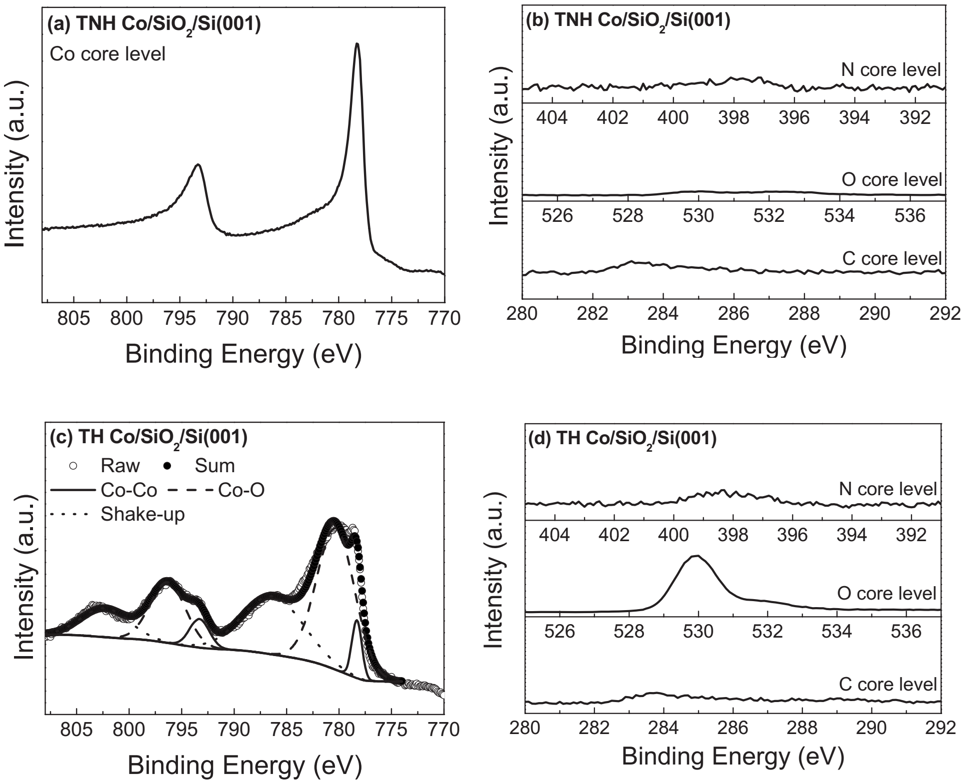

Figure 4. The XPS spectra of [(a) and (b)] TNH Co and [(c) and (d)] TH Co in Co core level and impurity content (N, O, and C) core levels, respectively.

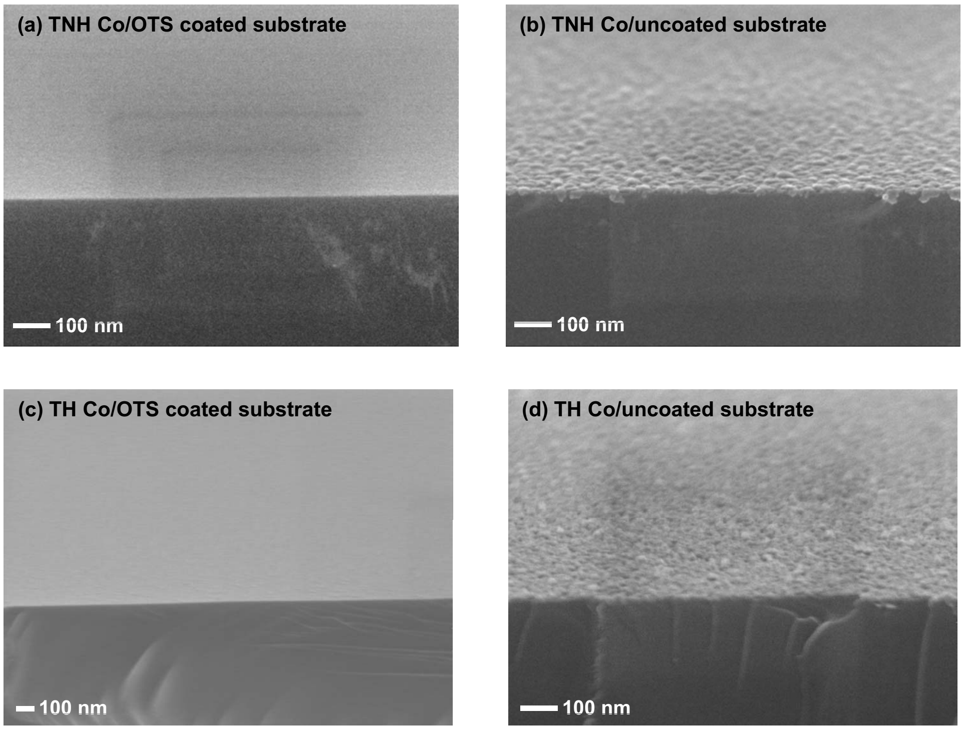

Figure 5. The FESEM images of [(a) and (b)] TNH Co films and [(c) and (d)] TH Co films on OTS-uncoated and -coated substrates, respectively.

data not shown), while 24 nm thick Co films were deposited onto the uncoated substrate (Fig. 5b). Figure 5c and d shows the SEM images of TH Co deposited onto the OTS-coated and -uncoated substrates, respectively, indicating that Co films are observed only on the uncoated substrate similar to the TNH Co case. These observations indicate that the OTS effectively blocks the Co film deposition during the Co TH-ALD, irrespective of the reactant.

Then, the Co AS-ALD was carried out using NH_3 at $T_s = 350°C$ and $t_r = 1$ s on a substrate with prepatterned OTS prepared by the sequences, as shown in Fig. 1. The line pattern was formed by conventional photolithography, composed of an alternative OTS-coated region (9 μm width) and -uncoated region (3 μm width). Figure 6a is an AFM image showing the morphology of Co films by TNH Co for 1000 cycles. The AFM image shows that the width of the Co lines and the distance between the lines are 3 and 9 μm, respectively, exactly replicating the inverse of the OTS pattern. The thickness profile of AS-ALD Co shows that the thickness difference between the highest point and the lowest point is 24 nm, which is the same thickness on the uncoated blank substrate (Fig. 6b). Thus, we infer that Co is only deposited onto the uncoated region without nucleation delay. Also, no deposition occurred on the OTS-coated region.

The quality of the AS-ALD Co film was estimated by current–voltage (*I-V*) measurement. When the electrical probes were placed on the same Co line with 100 μm of probe distance, a clear ohmic behavior was observed with a linear increase in current and with an increase in voltage, as Fig. 6c shows. The resistivity of the Co line was estimated to be 935 μΩ cm by assuming that the Co line is rectangular (cross-sectional area = 24 nm × 3 μm; length = 100 μm). The resistivity of the Co line calculated from *I-V* is higher than that of the TH-ALD Co film measured by a four-point probe. The resistivity increase is attributed mainly to contact resistance and spreading resistance caused by two-point probe measurements. The size effect may not be significant because we compare the resistivity of the line and film with the same thickness, and the width of the line is in the micrometer scale.[38,39] In contrast, no detectable current was measured on different Co lines, indicating that each Co line is electrically isolated, which shows that Co film is not formed on the OTS-coated region.

Figure 7a shows the thickness profile of TNH Co on the patterned OTS substrate for 2000 cycles. The thickness difference between the highest and lowest points was 32 nm, which is significantly smaller that the expected thickness (48 nm). In contrast to 1000 cycles, both of the *I-V* characteristics on the same and different Co lines show an ohmic behavior (Fig. 7b). The current detection between different Co lines indicates that each Co line is not electrically isolated. We observed 48 nm of Co on the OTS-free region and 16 nm of Co on the OTS-coated regions in SEM analysis, consistent with the profilometer and *I-V* results. Therefore, we infer that the Co was deposited even onto the OTS-coated region, reducing the thickness difference to 32 nm, as shown in Fig. 7a.

In previous reports on AS-ALD utilizing the SAM-blocking layer, the loss of deposition selectivity above a certain number of growth cycles is a common observation. For instance, in AS-ALD of Pt [40] and HfO_2 [31] using OTS as a blocking layer at $T_s = 285$ and 250°C, the selectivity of deposition was lost at longer process times than 25600 and 18015 s, respectively. Indeed, the hydrophobicity of the OTS-coated surface was reported to be thermally degraded below 200°C within a few minutes in air through the cleavages of the Si–C and C–C bondings.[41] In vacuum or other ambient, however, the degradation of OTS hydrophobicity is retarded to a higher temperature because the amount of chemical entity cleaving hydrocarbon chains of OTS such as water is very small.[42,43] There were reports that the degradation temperatures of OTS become even up to 400 and 470°C in N_2 ambient and ultrahigh vacuum, respectively.[42,43] Therefore, the loss of deposition selectivity with an increasing number of ALD cycles can be explained by the thermal degradation of OTS. In our AS-ALD, the loss of deposition selectivity was observed over 1000 cycles, namely, 6000 s of total time of the ALD process. Compared with that of Pt and HfO_2, the total process time until the loss of selective deposition is relatively short probably due to the higher growth temperature of 350°C.

Conclusion

In summary, Co T-ALD using a Co precursor, Co(iPr-AMD)$_2$, and two reactants, H_2 and NH_3, was investigated and applied to AS-ALD with OTS SAM as a blocking layer. Metal thin-film depo-

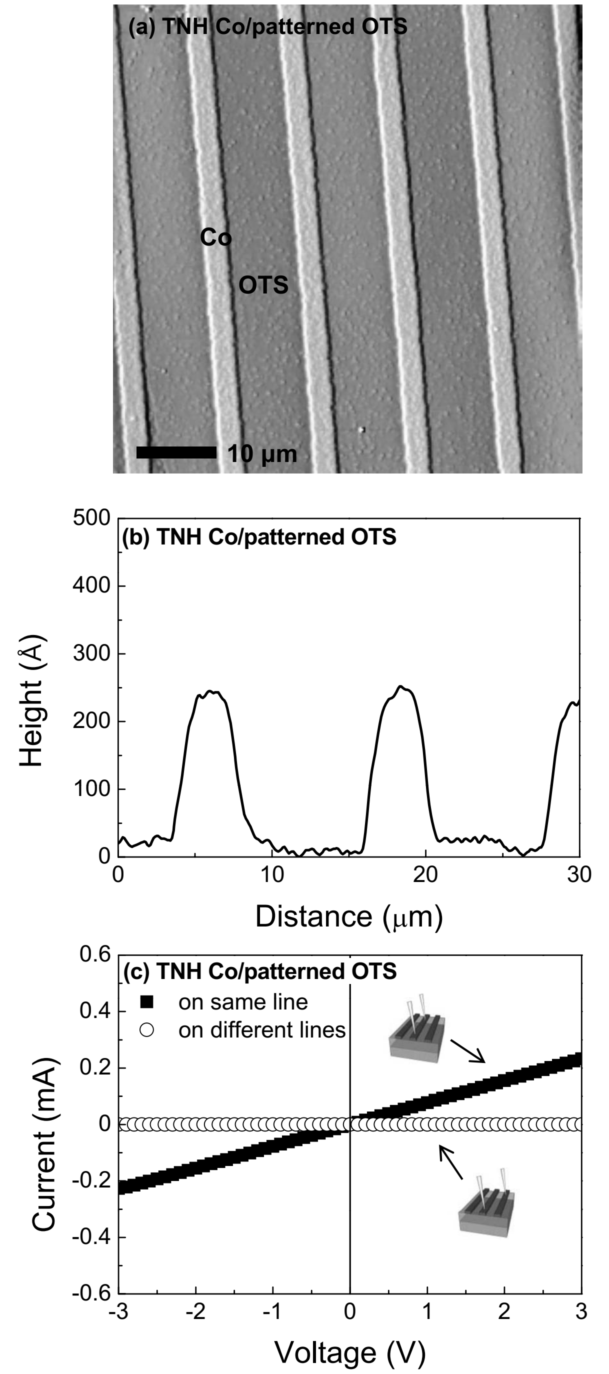

Figure 6. (a) The AFM image, (b) the thickness profile of TNH Co deposited onto patterned OTS-coated substrate for 1000 cycles, and (c) *I-V* results of AS-ALD Co on same lines (■) and different lines (○) (inset: Cartoons of probes on Co lines).

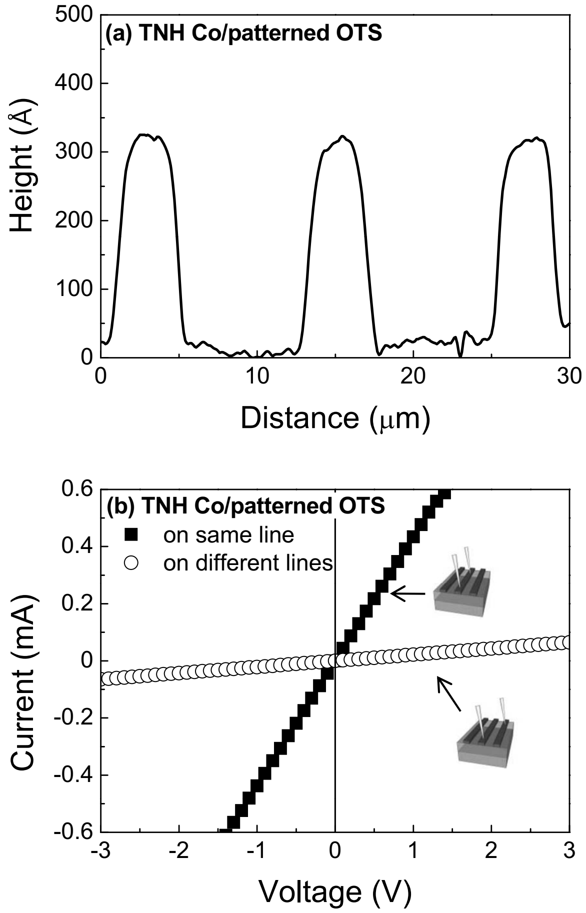

Figure 7. (a) The thickness profile of TNH Co deposited onto patterned OTS-coated substrate for 2000 cycles and (b) *I-V* results of AS-ALD Co on same lines (■) and different lines (○) (inset: Cartoons of probes on Co lines).

sition by T-ALD using NH_3 was reported, and the T-ALD Co from NH_3 showed superior film properties, lower resistivity, lower impurity level, and high density compared to that from H_2. Co AS-ALD was achieved by both Co T-ALD processes to 1000 cycles. Through the Co AS-ALD, 3 μm wide Co line patterns were obtained on a prepatterned OTS-coated substrate without an etching process.

Acknowledgments

This work was supported by the Korea Science and Engineering Foundation (KOSEF) grant funded by the Korean government (MOST) (no. 2007-02864 and no. R01-2007-000-20143-0). The synchrotron radiation XRR analysis was performed at the 3C2 X-ray scattering beam line of the Pohang Acceleration Laboratory (PAL).

Yonsei University assisted in meeting the publication costs of this article.

References

1. S. S. P. Parkin, N. More, and K. P. Roche, *Phys. Rev. Lett.*, **64**, 2304 (1990).
2. Q. Xiao, T. Yang, A. Ursache and M. T. Tuominen, *J. Appl. Phys.*, **103**, 07C521 (2008).
3. F. M. Yang, T. C. Chang, P. T. Liu, P. H. Yeh, Y. C. Yu, J. Y. Lin, S. M. Sze, and J. C. Lou, *Appl. Phys. Lett.*, **90**, 132102 (2007).
4. C.-J. Kim, S.-W. Ryu, Y.-K. Choi, J.-J. Chang, S. H. Bae, and B.-H. Sohn, *Appl. Phys. Lett.*, **93**, 052106 (2008).
5. H.-B.-R. Lee and H. Kim, *Electrochem. Solid-State Lett.*, **9**, G323 (2006).
6. H.-B.-R. Lee, J. Y. Son, and H. Kim, *Appl. Phys. Lett.*, **90**, 213509 (2007).
7. J. H. Lee and J. H. Cha, *Microelectron. Eng.*, **71**, 321 (2004).
8. W.-H. Kim, S.-J. Park, J.-Y. Son, and H. Kim, *Nanotechnology*, **19**, 045302 (2008).
9. M. Daub, M. Knez, U. Goesele and K. Nielsch, *J. Appl. Phys.*, **101**, 09J111 (2007).
10. E. Farm, M. Kernell, M. Ritala, and M. Leskel, *Chem. Vap. Deposition*, **12**, 415 (2006).
11. R. Chen and S. F. Bent, *Adv. Mater.*, **18**, 1086 (2006).
12. J. Huo, R. Solanki, and J. McAndrew, *J. Mater. Res.*, **17**, 2394 (2002).
13. J. W. Elam, A. Zinovev, C. Y. Han, H. H. Wang, U. Welp, J. N. Hryn, and M. J. Pellin, *Thin Solid Films*, **515**, 1664 (2006).
14. H. Kim and S. M. Rossnagel, *J. Vac. Sci. Technol. A*, **20**, 802 (2002).
15. H. Kim, C. Cabral, C. Lavoie, and S. M. Rossnagel, *J. Vac. Sci. Technol. B*, **20**, 1321 (2002).
16. O.-K. Kwon, S.-H. Kwon, H.-S. Park, and S.-W. Kang, *J. Electrochem. Soc.*, **151**, C753 (2004).
17. J. Chae, H. S. Park, and S. W. Kang, *Electrochem. Solid-State Lett.*, **5**, C64 (2002).
18. X. Jiang, H. Huang, F. B. Prinz, and S. F. Bent, *Chem. Mater.*, **20**, 3897 (2008).
19. C. Bae, H. Yoo, S. Kim, K. Lee, J. Kim, M. M. Sung, and H. Shin, *Chem. Mater.*, **20**, 756 (2008).

20. R. Chen, H. Kim, P. C. McIntyre, and S. F. Bent, *Appl. Phys. Lett.*, **84**, 4017 (2004).
21. J. P. Lee and M. M. Sung, *J. Am. Chem. Soc.*, **126**, 28 (2004).
22. R. Chen, H. Kim, P. C. McIntyre, and S. F. Bent, *Chem. Mater.*, **17**, 536 (2005).
23. R. Chen, H. Kim, P. C. McIntyre, D. W. Porter, and S. F. Bent, *Appl. Phys. Lett.*, **86**, 191910 (2005).
24. B. H. Lee and M. M. Sung, *J. Nanosci. Nanotechnol.*, **7**, 3758 (2007).
25. E. K. Seo, J. W. Lee, H. M. Sung-Suh, and M. M. Sung, *Chem. Mater.*, **16**, 1878 (2004).
26. K. J. Park, J. M. Doub, T. Gougousi, and G. N. Parsons, *Appl. Phys. Lett.*, **86**, 051903 (2005).
27. R. Chen and S. F. Bent, *Chem. Mater.*, **18**, 3733 (2006).
28. A. Dube, M. Sharma, P. F. Ma, and J. R. Engstrom, *Appl. Phys. Lett.*, **89**, 164108 (2006).
29. B. S. Lim, A. Rahtu, and R. G. Gordon, *Nature Mater.*, **2**, 749 (2003).
30. Z. Li, R. G. Gordon, D. B. Farmer, Y. Lin, and J. Vlassak, *Electrochem. Solid-State Lett.*, **8**, G182 (2005).
31. J. Hong, D. W. Porter, R. Sreenivasan, P. C. McIntyre, and S. F. Bent, *Langmuir*, **23**, 1160 (2007).
32. T. M. Mayer, M. P. de Boer, N. D. Shinn, P. J. Clews, and T. A. Michalske, *J. Vac. Sci. Technol. B*, **18**, 2433 (2000).
33. D. K. Schwartz, *Annu. Rev. Phys. Chem.*, **52**, 107 (2001).
34. J. F. Moulder, W. F. Stickle, P. E. Sobol, and K. D. Bomben, *Handbook of X-Ray Photoelectron Spectroscopy*, Perkin-Elmer, Eden Prairie, MN (1992).
35. M. Oku and K. Hirokawa, *J. Electron Spectrosc. Relat. Phenom.*, **8**, 475 (1976).
36. M. Burriel, G. Garcia, J. Santiso, A. Abrutis, Z. Saltyte, and A. Figueras, *Chem. Vap. Deposition*, **11**, 106 (2005).
37. H. Li, D. B. Farmer, R. G. Gordon, Y. Lin, and J. Vlassak, *J. Electrochem. Soc.*, **154**, D642 (2007).
38. W. Steinhögl, G. T. Schindler, G. Steinlesberger, and M. Engelhardt, *Phys. Rev. B*, **66**, 075414 (2002).
39. S. M. Rossnagel and T. S. Kuan, *J. Vac. Sci. Technol. B*, **22**, 240 (2004).
40. X. Jiang and S. F. Bent, *J. Electrochem. Soc.*, **154**, D648 (2007).
41. Y. X. Zhuang, O. Hansen, T. Knieling, C. Wang, P. Rombach, W. Lang, W. Benecke, M. Kehlenbeck, and J. Koblitz, *J. Micromech. Microeng.*, **16**, 2259 (2006).
42. G. J. Kluth, M. M. Sung, and R. Maboudian, *Langmuir*, **13**, 3775 (1997).
43. U. Srinivasan, M. R. Houston, R. T. Howe, and R. Maboudian, *J. Microelectromech. Syst.*, **7**, 252 (1998).